A 3D CONFORMING-NONCONFORMING MIXED FINITE ELEMENT FOR SOLVING SYMMETRIC STRESS STOKES EQUATIONS

MIN ZHANG AND SHANGYOU ZHANG

Abstract. We propose a 3D conforming-nonconforming mixed finite element for solving symmetric stress Stokes equations. The low-order conforming finite elements are not inf-sup stable. The low-order nonconforming finite elements do not satisfy the Korn inequality. The proposed finite element space consists of two conforming components and one nonconforming component. We prove that the discrete inf-sup condition is valid and the discrete Korn inequality holds uniformly in the mesh-size. Based on these results we give some numerical verification. In addition, this element is compared numerically with six other mixed finite elements.

Key words. Mixed finite element, symmetric stress, Korn's inequality, Stokes equations.

1. Introduction

Finite element methods for the 2D symmetric stress Stokes problem have been extensively studied in the literature, and most of stable schemes are summarized in book [6]. However, only little attention has been paid to the 3D problems. Actually, the nonconforming elements of Crouseix-Raviart [10] is only suitable if $\Gamma_N = \emptyset$ due to a missing Korn's inequality in two as well as in three dimensions. In 2D, the nonconforming elements of Kouhia and Stenberg [17] circumvent this problem by choosing one component nonconforming element and the other one conforming element. [19] has also given a counter example to show that if both of the two components are nonconforming rotated Q_1 elements, discrete Korn's inequality is invalid. From these works, we are hinted to use different spaces for different components of the velocity to assure the well-posedness of the discrete problem. We prove that the mixed finite elements with one nonconforming component, the nonconforming rotated Q_1 element, the conforming Q_2 element and the conforming Q_1 element for the other two components of the velocity, respectively, satisfy the discrete Korn inequality. In addition, such a velocity element combined with a piecewise constant pressure element, i.e., $RQ_1 \times Q_2 \times Q_1$-$P_0$, is inf-sup stable. For the nonconforming rotated Q_1 element, Rannacher and Turek analyzed this element in [23] for solving the (gradient) Stokes equations. The element has shown superconvergence in special meshes according to [18]. However, as mentioned above, this rotated Q_1 element does not satisfy the discrete Korn inequality and does not solve the symmetric stress Stokes equations (see numerical tests below.) Similarly, the Cai-Douglas-Santos-Sheen-Ye's element [7, 8, 11] does not work for the symmetric stress Stokes equations either. But the element can be used for one component of the velocity, replacing the rotated Q_1 element.

We note that, unlike the 2D case, two components of C^0-Q_1 of the velocity are not enough. That is, the $RQ_1 \times Q_1 \times Q_1$-$P_0$ mixed finite element does not solve the symmetric stress Stokes equations. A numerical test on the element is provided. The proposed $RQ_1 \times Q_2 \times Q_1$-$P_0$ is almost the simplest mixed finite

element. Here we can have another slightly simpler version of the proposed mixed finite elements that the conforming Q_2 can be replaced by the conforming $Q_{2,1,1}$ space, for example, where $Q_{1,2,1}$ denote the polynomials of separated degrees 2, 1 and 1. The analysis for this mixed finite element is same. Numerically, we test the newly proposed finite element, along with six other typical mixed finite elements, including this simplified element $RQ_1 \times Q_{2,1,1} \times Q_1$-$P_0$.

The rest of the paper is organized as follows. In section 2, we present the symmetric stress Stokes problem. In section 3, we define the conforming nonconforming combined mixed finite element. The well-posedness of the discrete problem and an error estimate will be proved for the proposed mixed finite element. Section 4 concludes this paper with seven numerical experiments.

Throughout this paper, standard notation on Lebesgue and Sobolev spaces is employed. $(\cdot, \cdot)$ denotes the L^2 scalar product over Ω. Let $\| \cdot \|_{0,\Omega}$ denote the L^2 norm over a set $\Omega \subset \Omega$ and $\| \cdot \|_0$ abbreviate $\| \cdot \|_{0,\Omega}$. $|\cdot|_{1,h}$ denotes the semi-H^1 norm for nonconforming functions and $|\cdot|_1$ the standard semi-H^1 norm. $\partial\Omega$ denotes the boundary of Ω. If there is no special instruction, the bold face letter will indicate a vector or vector space in order to distinguish it from scalars. Let $A \lesssim B$ abbreviates that there is some mesh-size independent generic constant $0 \leq \mathcal{C} \leq \infty$ such that $A \leq \mathcal{C}B$.

2. The symmetric stress Stokes problem

Assuming the domain $\Omega \in R^3$ is a convex, polyhedral, bounded Lipschitz domain, which can be triangulated by parallelepipeds (or simply by cuboids), with closed Dirichlet boundary Γ_D and Neumann boundary $\Gamma_N = \partial\Omega \setminus \Gamma_D$, both with non-zero two dimensional measure, and some right-hand side functions $\mathbf{f} \in [L^2(\Omega)]^3$, $\mathbf{u}_1 \in [H^{3/2}(\Gamma_D)]^3$ and $\mathbf{g} \in [H^{1/2}(\Gamma_N)]^3$, the three dimensional symmetric stress Stokes problem seeks the velocity $\mathbf{u} \in [H^1(\Omega)]^3$ and pressure $p \in L^2(\Omega)$ such that

$$
(1) \quad
\begin{cases}
-2\mu \operatorname{div} \varepsilon(\mathbf{u}) + \nabla p = \mathbf{f} & \text{in } \Omega \\
\operatorname{div} \mathbf{u} = 0 & \text{in } \Omega \\
\mathbf{u} = \mathbf{u}_D & \text{on } \Gamma_D \\
\sigma \mathbf{n} = \mathbf{g} & \text{on } \Gamma_N,
\end{cases}
$$

where, and throughout this paper, $\mathbf{n}$ is the unit normal vector on the boundary, $\mu > 0$ is the viscosity, $\sigma = (2\mu\varepsilon(\mathbf{u}) - pI)$, and $\varepsilon(\mathbf{u})$ is the symmetric gradient of a vector, which is

$$
\varepsilon(\mathbf{u}) = \frac{1}{2}(\nabla\mathbf{u} + \nabla\mathbf{u}^T)
$$

$$
= \frac{1}{2}
\begin{pmatrix}
2\partial_x u_1 & \partial_y u_1 + \partial_x u_2 & \partial_z u_1 + \partial_x u_3 \\
\partial_y u_1 + \partial_x u_2 & 2\partial_y u_2 & \partial_z u_2 + \partial_y u_3 \\
\partial_z u_1 + \partial_x u_3 & \partial_z u_2 + \partial_y u_3 & 2\partial_z u_3
\end{pmatrix}
$$

for any $\mathbf{u} = [u_1 \ u_2 \ u_3]^T \in [H^1(\Omega)]^3$.

We note that due to the boundary conditions, the symmetric stress Stokes problem (1) is not equivalent to a standard (gradient) Stokes problem.

The weak formulation of equation (1) reads Find $(\mathbf{u}, p) \in \mathbf{V} \times L^2(\Omega)$, such that

$$
(2) \quad
\begin{cases}
a(\mathbf{u}, \mathbf{v}) + b(p, \mathbf{v}) = (\mathbf{f}, \mathbf{v}) + \displaystyle\int_{\Gamma_N} \mathbf{g} \cdot \mathbf{v}\, ds & \forall \mathbf{v} \in \mathbf{V}_0, \\
b(q, \mathbf{u}) = 0 & \forall q \in L^2(\Omega),
\end{cases}
$$

where

$$\mathbf{V} = \{\mathbf{v} \in \mathbf{H}^1(\Omega) \mid \mathbf{v}|_{\Gamma_D} = \mathbf{u}_D\},$$

$$\mathbf{V}_0 = \{\mathbf{v} \in \mathbf{H}^1(\Omega) \mid \mathbf{v}|_{\Gamma_D} = 0\},$$

$$a(\mathbf{u}, \mathbf{v}) = 2\mu \int_\Omega \varepsilon(\mathbf{u}) : \varepsilon(\mathbf{v}) d\mathbf{x},$$

$$b(q, \mathbf{v}) = -\int_\Omega q \operatorname{div} \mathbf{v} \, d\mathbf{x}.$$

The well-posedness of (2) is ensured by a theorem from [6] and [23].

Theorem 2.1. *Then the weak problem* (2) *admits a unique solution* $(\mathbf{u}, p) \in \mathbf{V} \times L_0^2(\Omega)$ *such that*

(3) $\|\mathbf{u}\|_1 + \|p\|_0 \leq C\|\mathbf{f}\|_{-1} + C\|\mathbf{g}\|_{-1/2, \Gamma_N} + C\|\mathbf{u}_D\|_{1/2, \Gamma_D}.$

3. Finite element approximation

3.1. notations. Let $\mathcal{T}_h$ be regular and shape-regular decompositions of $\Omega \subset R^3$ into parallelepiped, or simply rectangular cubes, denoted by K, where the mesh parameter $h > 0$ describes the maximum diameter of the elements of $\mathcal{T}_h$. Let $\mathcal{F}$ be the set of all faces in $\mathcal{T}_h$. Given any face F with diameter h_F, we assign a unit normal vector $\mathbf{n}_F := (n_1, n_2, n_3)$ to the face. For an internal $F \in \mathcal{F}$, once $\mathbf{n}_F$ has been fixed on F, in relation to $\mathbf{n}_F$ one defines the elements $K_- \in \mathcal{T}_h$ and $K_+ \in \mathcal{T}_h$ with $F = K_- \cap K_+$. The jump of $\mathbf{u}$ across F is denoted by $[\mathbf{u}]_F := (\mathbf{u}|_{K_+})|_F - (\mathbf{u}|_{K_-})|_F$. The jump on the boundary faces $(\subset \partial\Omega)$ is defined similarly. Let $\widehat{K}$ be the reference cube with vertices $\widehat{Z}_i$, $1 \leq i \leq 8$. Then exists a unique invertible mapping G_K that maps $\widehat{K}$ onto K with $G_K(\xi, \eta, \gamma) \in Q_1^3(\xi, \eta, \gamma)$ and $G_K(\widehat{Z}_i) = Z_i$. Here ξ, η, γ are the local isoparametric coordinates. We denote by P_k the set of polynomials of degree less than or equal to k, and by Q_k the set of polynomials of degree less than or equal to k in each variable.

We introduce the conforming Q_1 element space

(4) $W_h = \{v \in H^1_{\Gamma_D}(\Omega) \mid \widehat{v}|_K \in Q_1(\widehat{K}) \quad \forall K \in \mathcal{T}_h\},$

where $H^1_{\Gamma_D}(\Omega) = \{v|_{\Gamma_D} = 0\} \cap H^1(\Omega)$, the conforming Q_2 element space

(5) $Z_h = \{v \in H^1_{\Gamma_D}(\Omega) \mid \widehat{v}|_K \in Q_2(\widehat{K}) \quad \forall K \in \mathcal{T}_h\},$

and the piecewise constant pressure space

(6) $Q_h = \{q \in L^2(\Omega) \mid q|_K \in P_0(K) \quad \forall K \in \mathcal{T}_h\}.$

The definition of nonconforming, rotated Q_1 element (RQ_1) space in 3D [23] is as follows. The shape function space is

$$RQ_1(K) = \left\{\widehat{v} \circ G_K^{-1} \mid \widehat{v} \in \operatorname{span}\{1, x, y, z, x^2 - y^2, x^2 - z^2\} \right\},$$

where G_K is the tri-linear mapping from $\widehat{K}$ to K. On a face $F \in \partial K$, we denote the average and the jump by

$$A_{F,K}(v) = \frac{1}{|F|} \int_F v \qquad \forall v \in H^1(K),$$

$$J_F(v) = \frac{1}{|F|} \int_F [v]_F \qquad \forall v \in H^1(\Omega).$$

The global RQ_1 space is

$$V_h^{RQ_1} = \left\{v \in L^2(\Omega) \mid v|_K \in RQ_1(K), \ K \in \mathcal{T}_h, ; \ J_F(v) = 0, \ F \in \mathcal{F} \cap \Omega\right\}.$$

With the boundary condition, the RQ_1 space is

$$V_{0,h}^{RQ_1} = \left\{ v \in V_h^{RQ_1} \mid A_{F,K}(v) = 0, \ \forall F \in \mathcal{F} \cap \Gamma_D \right\}.$$

In addition, we have to work with "piecewise" defined bilinear forms and corresponding norms

(7)
$$a_h(\mathbf{u}_h, \mathbf{v}_h) = 2\mu \sum_{K \in \mathcal{T}_h} \int_K \varepsilon(\mathbf{u}_h) : \varepsilon(\mathbf{v}_h) d\mathbf{x},$$

$$b_h(q, \mathbf{u}_h) = - \sum_{K \in \mathcal{T}_h} \int_K q_h \operatorname{div} \mathbf{v}_h d\mathbf{x}.$$

$$\|v\|_{l,h}^2 = \sum_{K \in \mathcal{T}_h} \|v\|_{l,K}^2, \quad |v|_{l,h}^2 = \sum_{K \in \mathcal{T}_h} |v|_{l,K}^2, \quad l = 1, 2.$$

The global finite element space for the velocity is defined by

(8)
$$\mathbf{V}_h = V_{0,h}^{RQ_1} \times Z_h \times W_h,$$

and the finite element pressure space is Q_h, defined in (6). Here, for $\mathbf{u}_h \in \mathbf{V}_h$, we have

$$\mathbf{u}_h = \begin{pmatrix} u_{h1} \\ u_{h2} \\ u_{h3} \end{pmatrix}, \quad u_{h1} \in V_{0,h}^{RQ_1}, \quad u_{h2} \in Z_h, \quad u_{h3} \in W_h.$$

For simplicity, we assume $\mathbf{u}_D = \mathbf{0}$ and $\Gamma_N = \emptyset$ in (1), in the finite element problem. The finite element method can be stated as: Find $(\mathbf{u}_h, p_h) \in \mathbf{V}_h \times Q_h$ such that

(9)
$$\begin{cases} a_h(\mathbf{u}_h, \mathbf{v}) + b_h(p_h, \mathbf{v}) = (\mathbf{f}, \mathbf{v}) & \forall \mathbf{v} \in \mathbf{V}_h, \\ b_h(q, \mathbf{u}_h) = 0 & \forall q \in Q_h, \end{cases}$$

Here $a_h(\mathbf{u}_h, \mathbf{v})$ and $b_h(q, \mathbf{u}_h)$ are defined in (7).

3.2. The BB inequality. We will prove the BB inequality for the finite element pair $(\mathbf{u}_h, p_h) \in \mathbf{V}_h \times Q_h$.

Theorem 3.1. *There is a constant $C > 0$, independent of h, such that*

(10)
$$\sup_{\mathbf{v} \in \mathbf{V}_h} \frac{b_h(p, \mathbf{v})}{\|\mathbf{v}\|_{1,h}} \geq C\|p\|_0 \qquad \forall p \in Q_h,$$

where $\mathbf{V}_h$ and Q_h are defined in (8) and (6), respectively.

Proof. The proof is done by a macro-element technique [17, 19]. Let M be a macro-element containing eight elements K_i and these elements share a common vertex which we denote as O, shown in Figure 1. We define the macro-space on such one macro-element.

$$\mathbf{V}_{0,M} = \{\mathbf{v} \in \mathbf{H}_0^1(M) \cap \mathbf{V}_h\},$$

$$P_M = \{p \in L_0^2(M) \cap Q_h\}.$$

Let the piecewise constant function be $p|_{K_j} = p_j$. We will show that if $b_h(p, \mathbf{v}) = 0$ for all $\mathbf{v} \in \mathbf{V}_{0,M}$, then all p_j are a global constant over M.

K_j is a cuboid for any $j = 1, 2, ..., 8$. Let the 12 internal faces of M be denoted by $F_i \in \mathcal{F}$, see Figure 1. Let the central points of each face F_i be denoted by O_i, $i = 1, 2, ...12$. According to Figure 1, let one of the four RQ_1 function v_1, the only non-vanishing freedom of $\mathbf{v}$, i.e., $\mathbf{v} = [v_1 \ 0 \ 0]^T$, be such that $\int_{F_i} v_1 = 1$ on one face
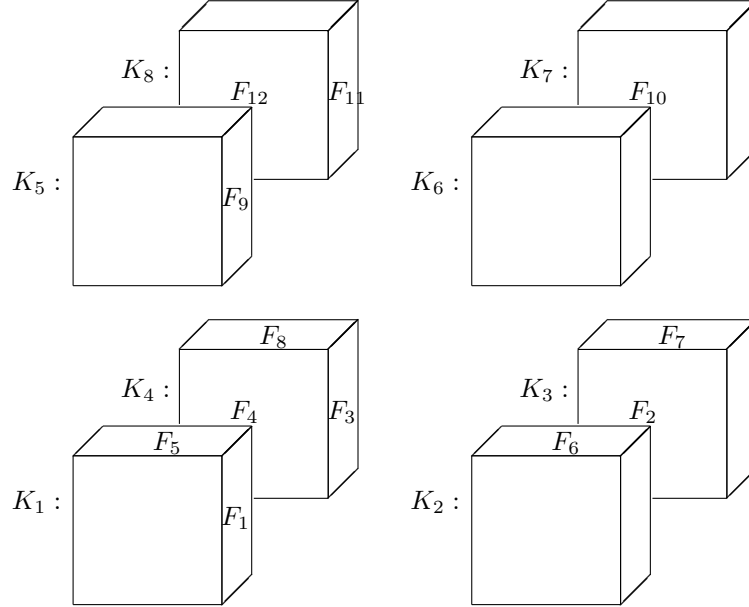
FIGURE 1.   Splitting a $2 \times 2 \times 2$ macro-element M of 8 cubes K_i, and 12 internal faces F_i.

F_i only, $i = 2, 4, 10, 12$, respectively. See Figure 1, the normal vectors of these four faces are parallel to the x-axis. For instance, when $i = 2$,

$$0 = b_h(p, \mathbf{v})_M = \int_{F_2} \mathbf{v} \cdot \mathbf{n}_2 \; p_2 dS - \int_{F_2} \mathbf{v} \cdot \mathbf{n}_2 \; p_3 dS$$
$$= \int_{F_2} v_1|_{K_2} p_2 \, dS - \int_{F_2} v_1|_{K_3} p_3 \, ds$$
$$= p_2 - p_3,$$

where $b_h(p, \mathbf{v})_M$ is defined in (7) on M. Hence $p_2 = p_3$. Repeating the computation on the other three faces, we get $p_4 = p_1$, $p_6 = p_7$ and $p_5 = p_8$.

Let the Q_2 function v_2, the only non-vanishing component of $\mathbf{v} = [0 \; v_2 \; 0]^T$, be such that $v_2(O_i) = 0$ is chosen that $\int_{F_i} v_2 = 1$, for $i = 1, 3, 9, 11$, respectively. When $i = 1$,

$$0 = b_h(p, \mathbf{v})_M = \int_{F_1} \mathbf{v} \cdot \mathbf{n}_1 p_1 \, dS - \int_{F_1} \mathbf{v} \cdot \mathbf{n}_1 \; p_2 \, dS$$
$$= p_1 - p_2.$$

We get $p_2 = p_1$. Then $p_3 = p_4$, $p_5 = p_6$ and $p_7 = p_8$. Combining the two results, we have, for some two constants a and b,

$$p_1 = p_2 = p_3 = p_4 = a,$$
$$p_5 = p_6 = p_7 = p_8 = b.$$

We next let $v_3 \in Q_1(M) \cap H_0^1(M)$ be the only non-vanishing degree of freedom, such that $v_3(O) = 1$, where O is the center of macro-element M.

$$0 = b_h(p, \mathbf{v})_M = \int_{F_5} \mathbf{v}|_{K_1} \cdot \mathbf{n}_5 \ a \ dS - \int_{F_5} \mathbf{v}|_{K_5} \cdot \mathbf{n}_5 \ b \ dS$$

$$+ \int_{F_6} \mathbf{v}|_{K_2} \cdot \mathbf{n}_6 \ a \ dS - \int_{F_6} \mathbf{v}|_{K_6} \cdot \mathbf{n}_6 \ b \ dS$$

$$+ \int_{F_7} \mathbf{v}|_{K_3} \cdot \mathbf{n}_7 \ a \ dS - \int_{F_7} \mathbf{v}|_{K_7} \cdot \mathbf{n}_7 \ b \ dS$$

$$+ \int_{F_8} \mathbf{v}|_{K_4} \cdot \mathbf{n}_8 \ a \ dS - \int_{F_8} \mathbf{v}|_{K_8} \cdot \mathbf{n}_8 \ b \ dS$$

$$= \frac{1}{3}|F_5|(a - b) + \frac{1}{3}|F_6|(a - b) + \frac{1}{3}|F_7|(a - b) + \frac{1}{3}|F_8|(a - b)$$

$$= \frac{1}{3}(|F_5| + |F_6| + |F_7| + |F_8|)(a - b).$$

Thus $a = b$. That is, the dimension of $(\operatorname{div} \mathbf{V}_{0,M})^\perp$ in P_h is 1. As we have (at least) one internal degree of freedom on each face, for each component of $\mathbf{v}$, by the macro-element technique of Stenberg [25], the inf-sup condition (10) holds. ∎

3.3. The discrete Korn inequality.

Lemma 3.1. *Let* $\mathbf{v}_h \in \mathbf{V}_h$. *For an internal point* $\mathbf{x}_0$ *of* $\mathcal{T}_h$, *let* $\Omega_{\mathbf{x}_0}$ *be the macro-element of eight cuboids sharing* $\mathbf{x}_0$ *as a central vertex. It holds that*

$$(11) \qquad \sum_{F \in \mathcal{F}(\Omega_{\mathbf{x}_0})} h_F^{-1} \|[\mathbf{v}_h]\|_{0,F}^2 \leq C \inf_{\mathbf{v} \in \mathbf{H}(\Omega_{\mathbf{x}_0})} \|\varepsilon_h(\mathbf{v} - \mathbf{v}_h)\|_{0,h,\Omega_{\mathbf{x}_0}}^2.$$

where $\mathbf{H}(\Omega_{\mathbf{x}_0}) := \{\mathbf{v} \in \mathbf{H}^1(\Omega_{\mathbf{x}_0}) \cap C^0(\Omega_{\mathbf{x}_0}) \mid \mathbf{v} = 0 \ on \ \partial\Omega_{\mathbf{x}_0}\}$, *and* C *is independent of* h.

Proof. The proof follows [14]. We prove (11) on the reference macro-element M, shown in Figure 1. Then (11) is obtained by the standard scaling argument.

Now, if $\|\varepsilon_h(\mathbf{v} - \mathbf{v}_h)\|_{0,h,\Omega_{\mathbf{x}_0}} = 0$ for some $\mathbf{v} \in \mathbf{H}(\Omega_{\mathbf{x}_0})$, the function $\mathbf{v} - \mathbf{v}_h$ is a rigid motion on each of eight K_i of M, because $\|\varepsilon_h(\mathbf{v} - \mathbf{v}_h)\|_{0,K_i} = 0$. That is,

$$(12) \qquad (\mathbf{v} - \mathbf{v}_h)_{K_i} = RM_{K_i} = \begin{pmatrix} a_i - e_i y - d_i z \\ b_i + e_i x - f_i z \\ c_i + d_i x + f_i y \end{pmatrix},$$

for some 48 constants, $a_i, b_i, c_i, d_i, e_i, f_i, i = 1, ..., 8$. Because $\mathbf{v} \in \mathbf{H}(\Omega_{\mathbf{x}_0})$ is continuous on $\Omega_{\mathbf{x}_0}$, and the second component and the third component of $\mathbf{v}_h$ are continuous (piecewise polynomials) on $\Omega_{\mathbf{x}_0}$, we have all eight constants of each group, $b_i, c_i, ..., f_i$, equal, on the whole $\Omega_{\mathbf{x}_0}$. We are left to show all eight a_i are equal. On the face F_1 between two cuboids K_1 and K_2 (cf. Figure 1), though $(\mathbf{v}_h)_1$ is not continuous, its face-integral is continuous. So the integral of the jump is zero. As $\mathbf{v} \in \mathbf{H}(\Omega_{\mathbf{x}_0})$ is continuous on F_1,

$$0 = \int_{F_1} [\mathbf{v}_1 - (\mathbf{v}_h)_1] = \int_{F_1} (\mathbf{v} - \mathbf{v}_h)_1|_{K_1} - (\mathbf{v} - \mathbf{v}_h)_1|_{K_2}$$

$$= \int_{F_1} (a_1 - a_2 - (e_1 - e_2)y - (d_1 - d_2)z) dS$$

$$= \int_{F_1} (a_1 - a_2) dS = (a_1 - a_2)|F_1|.$$

This leads to $a_1 = a_2$. Repeating this computation on F_2, F_3, F_8, F_9, F_{12} and F_{10} (see Figure 1), we show all eight a_i equal, on the whole $\Omega_{\mathbf{x}_0}$.

We conclude that $\mathbf{v} - \mathbf{v}_h$ in (12) is a global rigid motion, i.e., continuous across all internal faces, $\mathcal{F}(\Omega_{\mathbf{x}_0})$. So $\mathbf{v}_h$ is continuous in $\Omega_{\mathbf{x}_0}$, and

$$\sum_{F \in \mathcal{F}(\Omega_{\mathbf{x}_0})} \|[\mathbf{v}_h]\|_{0,F}^2 = 0.$$

Therefore (11) holds with $C > 0$ on the reference macro-element, because $\mathbf{v}_h$ is in a space of finite dimension. The general case follows from a scaling argument that the constant C in (11) is unchanged in the scaling transformation, i.e., independent of h. ∎

Theorem 3.2. *There is a positive constant C independent of the mesh size h such that*

$$(13) \qquad \|\mathbf{v}_h\|_{1,h} \le C\|\varepsilon_h(\mathbf{v}_h)\|_0 \qquad \forall \mathbf{v}_h \in \mathbf{V}_h.$$

Proof. First, according to the definition of the finite element space and results in [2, (1.5)], we have the following Poincaré inequality,

$$(14) \qquad \|\mathbf{v}_h\|_0^2 \lesssim \|\nabla_h \mathbf{v}_h\|_0^2 + |\int_{\Gamma_D} \mathbf{v}_h dS|^2 \lesssim \|\nabla_h \mathbf{v}_h\|_0^2 + \|\mathbf{v}_h\|_{0,\Gamma_D}^2.$$

By Lemma 3.1 and the discrete Korn inequality in [3, (1.19)],

$$\|\mathbf{v}_h\|_0^2 + \|\nabla_h \mathbf{v}_h\|_0^2$$
$$\lesssim \|\nabla_h \mathbf{v}_h\|_0^2 + \|\mathbf{v}_h\|_{0,\Gamma_D}^2$$
$$\lesssim \|\varepsilon_h(\mathbf{v}_h)\|_0^2 + \sum_{F \in \mathcal{F}(\Omega) \cup \mathcal{F}(\Gamma_D)} h_F^{-1}\|[\mathbf{v}_h]\|_{0,F}^2 + \|\mathbf{v}_h\|_{0,\Gamma_D}^2$$
$$\lesssim \|\varepsilon(\mathbf{v}_h)\|_0^2 + \sum_{F \in F(\Omega) \cup F(\Gamma_D)} h_F^{-1}\|[\mathbf{v}_h]_F\|_{0,F}^2$$
$$\lesssim \|\varepsilon(\mathbf{v}_h)\|_0^2 + \sum_{\text{internal vertex } \mathbf{x}_0} \inf_{\mathbf{v} \in \mathbf{H}(\Omega_{\mathbf{x}_0})} \|\varepsilon_h(\mathbf{v} - \mathbf{v}_h)\|_{0,h,\Omega_{\mathbf{x}_0}}^2$$
$$\lesssim \|\varepsilon(\mathbf{v}_h)\|_0^2 + \inf_{\mathbf{v} \in \mathbf{H}(\Omega)} \|\varepsilon_h(\mathbf{v} - \mathbf{v}_h)\|_{0,h}^2$$
$$\le \|\varepsilon(\mathbf{v}_h)\|_0^2 + \|\varepsilon_h(I_h \mathbf{v}_h - \mathbf{v}_h)\|_{0,h}^2$$
$$\lesssim \|\varepsilon(\mathbf{v}_h)\|_0^2 + \|\varepsilon_h(I_h \mathbf{v}_h)\|_{0,h}^2$$
$$\lesssim \|\varepsilon(\mathbf{v}_h)\|_0^2.$$

Here $\mathbf{H}(\Omega) = [H_0^1(\Omega) \cap C^0(\Omega)]^3$, and $I_h : \mathbf{V}_h \to \tilde{\mathbf{V}}_h \subset \mathbf{H}(\Omega)$ is the averaging interpolation operator, where

$$\tilde{\mathbf{V}}_h = W_h(C^0\text{-}Q_1) \times Z_h \times W_h.$$

That is, I_h averages a rotated Q_1 function $(\mathbf{v}_h)_1$ to a continuous Q_1 function. Such an operator is H^1 stable and symmetric-gradient stable, i.e.,

$$\|I_h \mathbf{v}_h\|_{1,h} \lesssim \|\mathbf{v}_h\|_{1,h}, \quad \|\varepsilon(I_h \mathbf{v}_h)\|_0 \lesssim \|\varepsilon_h(\mathbf{v}_h)\|_{0,h}.$$

∎

3.4. Error analysis.

Theorem 3.3. *Let* $(\mathbf{u}, p) \in \mathbf{H}^2(\Omega) \times H^1(\Omega)$ *be the solution of the variational problem (2). The problem (9) admits a unique solution* $(\mathbf{V}_h, Q_h)$ *such that*

$$(15) \qquad |\mathbf{u} - \mathbf{u}_h|_{1,h} + \|p - p_h\|_0 \le Ch\{\|\mathbf{u}\|_2 + |p|_1\},$$

$$(16) \qquad \|\mathbf{u} - \mathbf{u}_h\|_0 + \|p - p_h\|_{-1} \le Ch^2\{\|\mathbf{u}\|_2 + |p|_1\}.$$

Proof. Because the bilinear form $a_h(\cdot, \cdot)$ is coercive on $\mathbf{V}_h$, and because the inf-sup condition (10) holds, by the framework of mixed formulation [6], the problem (9) has a unique solution. Further, due to the inf-sup stability (10) and the consistent error control [2, 23], such a solution is quasi-optimal that

$$|\mathbf{u} - \mathbf{u}_h|_{1,h} + \|p - p_h\|_0 \lesssim (\inf_{\mathbf{v}_h \in \mathbf{V}_h} |\mathbf{u} - \mathbf{v}_h|_{1,0} + \inf_{q_h \in Q_h} \|p - q_h\|_0).$$

So (15) follows. The L^2 error estimate (16) follows by the standard duality argument [6]. ∎

4. Numerical experiments
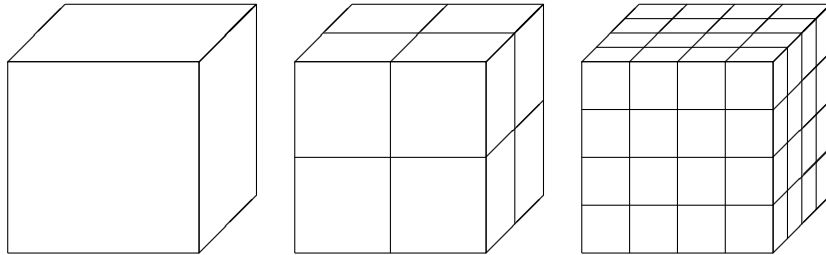
FIGURE 2. The first three levels of grids, $\mathcal{T}_1, \mathcal{T}_2$ and $\mathcal{T}_3$.

We solve the following symmetric stress Stokes equations

$$(17) \qquad \begin{cases} -\operatorname{div}\varepsilon(\mathbf{u}) + \nabla p = \mathbf{f} & \text{in } \Omega = (0,1)^3, \\ \operatorname{div}\mathbf{u} = 0 & \text{in } \Omega, \\ (\varepsilon(\mathbf{u}) - pI)\mathbf{n} = \mathbf{0} & \text{on } \Gamma_N = \{z = 1\} \cap \partial\Omega, \\ \mathbf{u} = \mathbf{0} & \text{on } \Gamma_D = \partial\Omega \setminus \Gamma_N, \end{cases}$$

where $\mathbf{f}$ is defined by the exact solutions

$$(18) \qquad \mathbf{u} = \mathbf{curl} \begin{pmatrix} y^2(1-y)^2 x(1-x)z^2(1-z)^3 \\ x^2(1-x)^2 y(1-y)z^2(1-z)^3 \\ 0 \end{pmatrix},$$

$$(19) \qquad p = (x - 1/2)(y - 1/2)(1 - z).$$

The first level grid is the domain itself. We refine each cube into 8 half-sized cubes to obtain next grid. Shown in Figure 2, the first three levels of grids, with grid size $h = 1, 1/2$ and $1/4$, respectively.

TABLE 1. The errors and the order of convergence by the $Q_2 \times Q_1 \times RQ_1 - P_0$ element.

level	$\|\mathbf{u} - \mathbf{u}_h\|_0$	h^n	$|\mathbf{u} - \mathbf{u}_h|_{1,h}$	h^n	$\|p - p_h\|_0$	h^n	$\dim \mathbf{V}_h$
2	0.001955	0.0	0.0141	0.0	0.01722	0.0	188
3	0.000872	1.2	0.0111	0.3	0.00838	1.0	1094
4	0.000272	1.7	0.0065	0.8	0.00308	1.4	7370
5	0.000074	1.9	0.0034	0.9	0.00098	1.6	53906
6	0.000019	1.9	0.0017	1.0	0.00029	1.8	411938
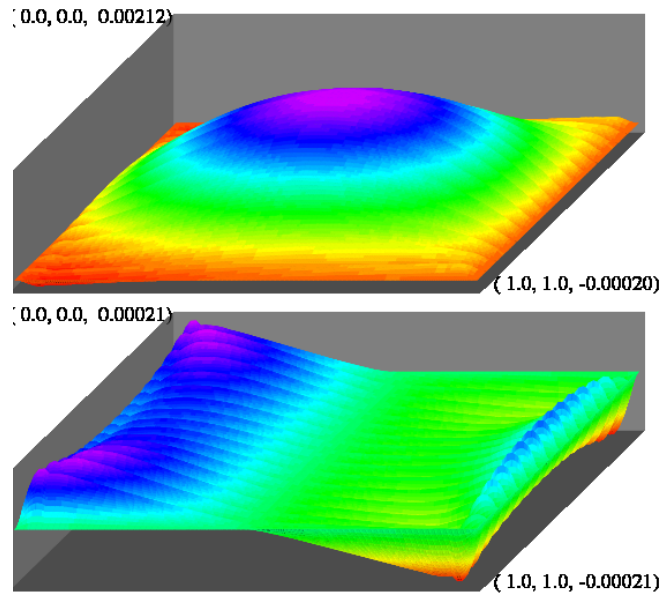
FIGURE 3. The computed $(\mathbf{u}_h)_1$, and the error, by Q_2, for (18) on the fifth grid.

TABLE 2. The errors and the order of convergence by the $Q_{1,1,2} \times Q_1 \times RQ_1 - P_0$ element.

level	$\|\mathbf{u} - \mathbf{u}_h\|_0$	h^n	$|\mathbf{u} - \mathbf{u}_h|_{1,h}$	h^n	$\|p_I - p_h\|_0$	h^n	$\dim \mathbf{V}_h$
2	0.000584	0.0	0.0040	0.0	0.09217	0.0	108
3	0.000519	0.2	0.0076	0.0	0.03827	1.3	590
4	0.000157	1.7	0.0043	0.8	0.01728	1.1	3834
5	0.000042	1.9	0.0022	1.0	0.00821	1.1	27506
6	0.000011	2.0	0.0011	1.0	0.00400	1.0	208098

4.1. The $Q_2 \times Q_1 \times RQ_1 - P_0$ mixed finite element. We use $C^0 - Q_2 \times C^0 - Q_1 \times RQ_1$ finite elements for the three components of the velocity $\mathbf{u}_h$. The pressure finite element space is the space of piecewise P_0 polynomials. The resulting linear systems of equations is solved by an iterative Uzawa method, stopping when the p_h update is less than 10^{-6}. In Table 1, we list the errors and the orders of convergence of the finite element solutions. The optimal order of convergence is achieved in the computation, as predicted by the theory.
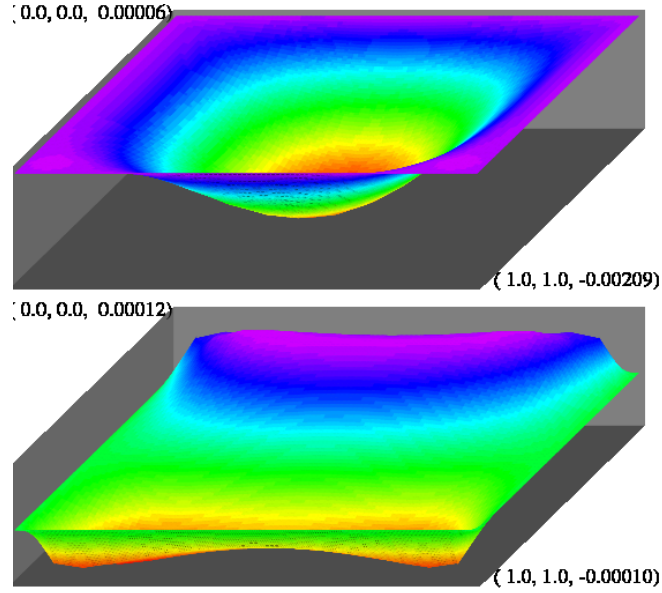
FIGURE 4. The computed $(\mathbf{u}_h)_2$, and the error, by Q_1, for (18) on the fifth grid.
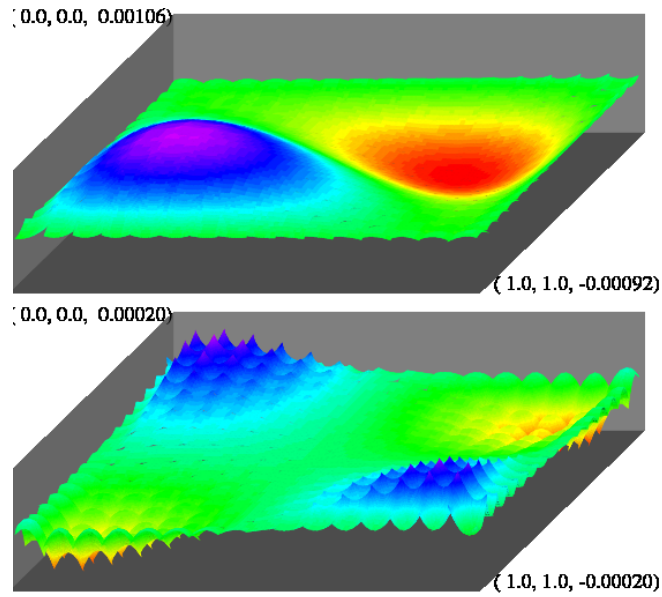
FIGURE 5. The computed $(\mathbf{u}_h)_3$, and the error, by RQ_1, for (18) on the fifth grid.

To compare the approximation power of different spaces of the three components of the velocity, we plot the finite element solution, and the error, cut on the plane $z = 0.2$, on the fifth grid, for the three components of $\mathbf{u}_h$ and for the pressure p_h, in Figures 3 – 6.
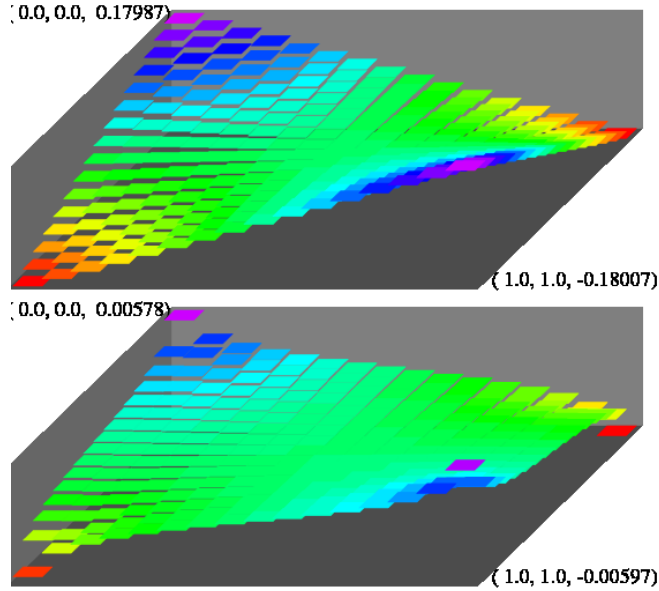
FIGURE 6. The computed p_h, and the error, by P_0, for (18) on the fifth grid.

4.2. The $Q_{1,1,2} \times Q_1 \times RQ_1 - P_0$ mixed finite element. We use $C^0 - Q_{1,1,2} \times C^0 - Q_1 \times RQ_1$ finite elements for the three components of the velocity $\mathbf{u}_h$. The pressure finite element space is the space of piecewise P_0 polynomials. Exactly the same proof of this paper would show that such a mixed finite element is inf-sup stable, and satisfies Korn's inequality. In Table 2, we list the errors and the orders of convergence of the finite element solutions. The optimal order of convergence is achieved in the computation.

This element is slightly simpler than the one in the last subsection. The total number of unknowns is about half of that. However, the approximation is about twice as good as the last one. Well, due to a loss of symmetry, the pressure solution is worse.

TABLE 3. The errors and the order of convergence by the conforming $Q_2 \times Q_2 \times Q_2 - P_0$ element.

level	$\|\mathbf{u} - \mathbf{u}_h\|_0$	h^n	$\|\mathbf{u} - \mathbf{u}_h\|_{1,h}$	h^n	$\|p_I - p_h\|_0$	h^n	$\dim \mathbf{V}_h$
2	0.002364	0.0	0.02307	0.0	0.01256	0.0	375
3	0.001011	1.2	0.01504	0.6	0.00775	0.7	2187
4	0.000328	1.6	0.00832	0.9	0.00317	1.3	14739
5	0.000092	1.8	0.00434	0.9	0.00106	1.6	107811
6	0.000024	1.9	0.00221	1.0	0.00032	1.7	823875

4.3. The conforming $Q_2 \times Q_2 \times Q_2 - P_0$ mixed finite element. We use $C^0 - Q_2 \times C^0 - Q_2 \times C^0 - Q_2$ finite elements for the three components of the velocity $\mathbf{u}_h$. The pressure finite element space is the space of piecewise P_0 polynomials. For such a mixed finite element pair, both the inf-sup condition and the discrete Korn inequality hold. However, due to the P_0 approximation of the pressure, only first order of convergence can be achieved for the Q_2 finite element functions. In Table

3, we list the errors and the orders of convergence of the finite element solutions. The optimal order of convergence is achieved in the computation, as predicted by the theory.

TABLE 4. The errors and the order of convergence by the conforming $Q_1 \times Q_1 \times Q_1 - P_0$ element.

level	$\|\mathbf{u} - \mathbf{u}_h\|_0$	h^n	$\|\mathbf{u}_I - \mathbf{u}_h\|_1$	h^n	$\|p_I - p_h\|_0$	h^n	$\dim \mathbf{V}_h$
2	0.000266	0.0	0.001593	0.0	0.03502	0.0	81
3	0.000178	0.6	0.001345	0.2	0.00902	2.0	375
4	0.000058	1.6	0.000449	1.6	0.00226	2.0	2187
5	0.000015	1.9	0.000121	1.9	0.00057	2.0	14739
6	0.000004	2.0	0.000031	2.0	0.00016	1.8	107811

4.4. The $Q_1 \times Q_1 \times Q_1 - P_0$ mixed finite element. We use $C^0 - Q_1 \times C^0 - Q_1 \times C^0 - Q_1$ finite elements for the three components of the velocity $\mathbf{u}_h$. The pressure finite element space is the space of piecewise P_0 polynomials. This mixed finite element is not inf-sup stable, but does satisfy the discrete Korn inequality. Although the element is not inf-sup stable, due to a super-convergence property [21, 22], such a mixed finite element even converges one order higher than the best approximation order. In Table 4, we list the errors and the orders of convergence of the finite element solutions. Again, though this element is not stable, it is the best element computing the symmetric stress Stokes equation. We note that the linear systems of equations here are solved iteratively. Otherwise we need to filter out the checkerboard modes of the pressure, when using the direct Gaussian elimination.

TABLE 5. The errors and the order of convergence by the $C^0 - Q_1 \times C^0 - Q_1 \times RQ_1 - P_0$ element.

level	$\|\mathbf{u} - \mathbf{u}_h\|_0$	h^n	$\|\mathbf{u}_I - \mathbf{u}_h\|_1$	h^n	$\|p_I - p_h\|_0$	h^n	$\dim \mathbf{V}_h$
1	0.000000	0.0	0.000000	0.0	0.00000	0.0	22
2	0.000793	0.0	0.005153	0.0	0.03753	0.0	90
3	0.001111	0.0	0.011705	0.0	0.02442	0.6	490
4	0.001182	0.0	0.011366	0.0	0.01665	0.6	3186
5	0.001272	0.0	0.011442	0.0	0.01359	0.3	22882

4.5. The $Q_1 \times Q_1 \times RQ_1 - P_0$ mixed finite element. We use $C^0 - Q_1 \times C^0 - Q_1 \times RQ_1$ finite elements for the three components of the velocity $\mathbf{u}_h$. The pressure finite element space is the space of piecewise P_0 polynomials. This mixed finite element does not satisfy the inf-sup condition. So the element solution does not converge, see Table 5.

4.6. The $Q_1 \times RQ_1 \times RQ_1 - P_0$ mixed finite element. We use $C^0 - Q_1 \times RQ_1 \times RQ_1$ finite elements for the three components of the velocity $\mathbf{u}_h$. The pressure finite element space is the space of piecewise P_0 polynomials. This mixed finite element does not satisfy the discrete Korn inequality. The finite element solution does not converge, cf. Table 6.

TABLE 6. The errors and the order of convergence by the $C^0 - Q_1 \times RQ_1 \times RQ_1 - P_0$ element.

level	$\|\mathbf{u} - \mathbf{u}_h\|_0$	h^n	$\|\mathbf{u}_I - \mathbf{u}_h\|_1$	h^n	$\|p_I - p_h\|_0$	h^n	dim $\mathbf{V}_h$
1	0.000000	0.0	0.0000	0.0	0.00000	0.0	20
2	0.000280	0.0	0.0063	0.0	0.02212	0.0	99
3	0.001892	0.0	0.0198	0.0	0.02748	0.0	605
4	0.001812	0.1	0.0211	0.0	0.02667	0.0	4185
5	0.001712	0.1	0.0210	0.0	0.02635	0.0	31025

TABLE 7. The errors and the order of convergence by the non-conforming $RQ_1 \times RQ_1 \times RQ_1 - P_0$ element.

level	$\|\mathbf{u} - \mathbf{u}_h\|_0$	h^n	$\|\mathbf{u} - \mathbf{u}_h\|_{1,h}$	h^n	$\|p - p_h\|_0$	h^n	dim $\mathbf{V}_h$
2	1114981.2	0.0	0.0780	0.0	0.0458	0.0	108
3	1649984.0	0.0	0.1862	0.0	0.0520	0.0	720
4	17973.8	6.5	0.0691	1.4	0.0501	0.1	5184
5	1092.8	4.0	0.0731	0.0	0.0508	0.0	39168

4.7. The non-conforming $RQ_1 \times RQ_1 \times RQ_1 - P_0$ mixed finite element. We use non-conforming $RQ_1 \times RQ_1 \times RQ_1$ finite elements for the three components of the velocity $\mathbf{u}_h$. The pressure finite element space is the space of piecewise P_0 polynomials. This mixed finite element is inf-sup stable, but it does not satisfy the discrete Korn inequality. In Table 7, we list the errors and the orders of convergence of the finite element solutions. Due to the failure of Korn's inequality, this mixed finite element does not work.

References

[1] J. H. Bramble and J. T. King. A robust finite element method for nonhomogeneous Dirichlet problems in domains with curved boundaries. Math. Comp. 63 (1994), no. 207, 1–17.
[2] S. C. Brenner. Poincaré-Friedrichs Inequalities for Piecewise H1 Functions. Numer. Funct. Anal. Optim. 25 (2004), no. 5, 463–478.
[3] S. C. Brenner. Korn's inequalities for piecewise H1 vector fields. Math. Comp. 73 (2004), no. 247, 1067–1087.
[4] S.C. Brenner and L.R. Scott. The Mathematical Theory of Finite Element Methods. Springer-Verlag, New York, 1994.
[5] H. Brezis. Functional analysis, Sobolev spaces and partial differential equations. Springer, New York, 2011.
[6] F. Brezzi and M. Fortin. Mixed and hybrid finite element methods. Springer Series in Computational Mathematics, 15. Springer-Verlag, New York, 1991.
[7] Z. Cai, J. Douglas, Jr., and X. Ye. A stable nonconforming quadrilateral finite element method for the stationary Stokes and Navier-Stokes equations. Calcolo 36 (1999), no. 4, 215–232.
[8] Z. Cai, J. Douglas, Jr., J.E. Santos, D. Sheen and X. Ye. Nonconforming quadrilateral finite elements: a correction. Calcolo 37 (2000), no. 4, 253–254.
[9] P. G. Ciarlet. The finite element method for elliptic problems. Studies in Mathematics and its Applications, Vol. 4. North-Holland Publishing Co., Amsterdam-New York-Oxford, 1978.

[10] M. Crouzeix and P. A. Raviart. Conforming and nonconforming finite element methods for solving the stationary Stokes equations. RAIRO R-3 (1973), 33–75.

[11] J. Douglas, J.E. Santos, D. Sheen and X. Ye. Nonconforming Galerkin methods based on quadrilateral elements for second order elliptic problems. M2AN Math. Model. Numer. Anal. 33 (1999), no. 4, 747–770.

[12] T. Dupont. L2 error estimates for projecting methods for parabolic equations in approximating domains. Mathematical Aspects of Finite Elements in Partial Differential Equations, C. de Boor, ed., Academic Press, New York, 1974, 313–352.

[13] H. Han. Nonconforming elements in the mixed finite element method. J. Comput. Math. 2 (1984), 223–233.

[14] J. Hu and M. Schedensack. A linear nonconforming finite element method for the Stokes flow in three dimensional space. Preprint.

[15] J. Hu and Z. Shi. Two lower order nonconforming quadrilateral elements for the Reissner-Mindlin plate. Science in China Series A: Mathematics 51 (2008), no. 11, 2097–2114.

[16] J. Hu and S. Zhang. Nonconforming finite element methods on quadrilateral meshes. Science China Mathematics 56 (2013), no. 12, 2599–2614.

[17] R. Kouhia and R. Stenberg. A linear nonconforming finite element method for nearly incompressible elasticity and Stokes flow. Comput. Methods Appl. Mech. Engrg. 124 (1995), no. 3, 195–212.

[18] Q. Lin, L. Tobiska and A. Zhou. Superconvergence and extrapolation of non-conforming low order finite elements applied to the Poisson equation. IMA Journal of Numerical Analysis 25 (2005), no. 1, 160–181.

[19] P. Ming and Z. Shi. Nonconforming rotated element for reissner-mindlin plate. Mathematical Models and Methods in Applied Sciences 11 (2001), no. 8, 1311–1342.

[20] P. Ming and Z. Shi. Quadrilateral mesh. Chin. Ann. Math. 23 (2002), no. 2, 235–252.

[21] J. Qin and S. Zhang. On the selective local stabilization of the mixed Q1-P0 element. Int. J. for Numerical Methods in Fluids 55 (2007), 1121–141.

[22] J. Qin and S. Zhang. Stability of the finite elements 9/(4c+1) and 9/5c for stationary Stokes equations. Computers and Structures 84 (2005), 70–77.

[23] R. Rannacher and S. Turek. Simple nonconforming quadrilateral Stokes element. Numer. Methods Partial Differential Equations 8 (1992), no. 2, 97–111.

[24] Z. Shi and M. Wang. Finite element methods. Science Press, Beijing, 2013.

[25] R. Stenberg. Analysis of mixed finite elements methods for the Stokes problem: a unified approach. Math. Comp. 42 (1984), no. 165, 9–23.

[26] X. Xu. On the Accuracy of Nonconforming Quadrilateral Q1 Element Approximation for the Navier–Stokes Problem. SIAM J. Numer. Anal. 38 (2000), no. 1, 17–39.

[27] Z. Zhang. Analysis of some quadrilateral nonconforming elements for incompressible elasticity. SIAM J. Numer. Anal. 34 (1997), no. 2, 640–663.

School of Mathematics, Sichuan University, Chengdu, China.
E-mail: 781068693@qq.com

Department of Mathematical Sciences, University of Delaware, Newark, DE 19716, USA.
E-mail: szhang@udel.edu